DEUTSCHES ELEKTRONEN-SYNCHROTRON DESY

DESY SR 86-08
October 1986

THREE-BEAM X-RAY STANDING WAVE ANALYSIS: A TWO DIMENSIONAL DETERMINATION OF ATOMIC POSITIONS

by

N. Greiser

Max-Planck-Institut für Festkörperphysik, Stuttgart

G. Materlik

Hamburger Synchrotronstrahlungslabor HASYLAB at DESY

ISSN 0723-7979

NOTKESTRASSE 85 · 2 HAMBURG 52

To be sure that your preprints are promptly included in the
HIGH ENERGY PHYSICS INDEX ,
send them to the following address (if possible by air mail) :

DESY
Bibliothek
Notkestrasse 85
2 Hamburg 52
Germany

DESY SR 86-08
October 1986

ISSN 0723-7979

THREE-BEAM X-RAY STANDING WAVE ANALYSIS: A TWO DIMENSIONAL DETERMINATION OF ATOMIC POSITIONS

N. Greiser

Max-Planck-Institut für Festkörperforschung,

Heisenbergstr. 1, 7000 Stuttgart 80, W. Germany

G. Materlik

Hamburger Synchrotronstrahlungslabor HASYLAB at DESY,

Notkestr. 85, 2000 Hamburg 52, W. Germany

Abstract

Measurements with X-ray standing wavefields were carried out for the first time in a three-beam diffraction geometry for Ge(400)(333)(115). The experimental results and the analysis using the dynamical multi-beam theory show that two independent Fourier components of the atomic density function can be determined simultaneously. This opens the way to a two dimensional position analysis of atoms in the bulk and on the surface of a single crystal.

submitted to Zeitschrift f. Physik

1. Introduction

The dynamical theory of x-ray diffraction /1,2/ predicts that, in a single crystal, standing x-ray wavefields are created which change their phases relative to the diffraction planes when passing the region of strong Bragg reflections. This effect has been used in experiments with x-ray standing wavefields to determine specific (e.g. those selected by their emitted fluorescence radiation) atomic distributions in the bulk /3,4,5/ or on surfaces /4,6,7/ of single crystals. A brief review of recent applications in combination with synchrotron radiation is given in /8/.

All X-ray standing wave (XSW) experiments so far have used a 2-beam case where only two wave vectors (K_0 incident, $\underline{K}_H$ reflected, $\underline{K}_H = \underline{K}_0 + \underline{H}$, $\underline{H} = (hkl)$ reciprocal lattice vector) are lying close to reciprocal lattice points (Ewald construction). This means reflection from one set of diffraction planes (hkl). In this case planes of constant E-field intensity (e.g. nodal and antinodal planes) are lying parallel to the diffraction planes with the same periodicity $d_{hkl} = 1/|\underline{H}|$. They move by ~ 0.5 d_{hkl} in direction $-\underline{H}$, when the Bragg reflection is crossed from low to high angle side. The fluorescence yield from an atom is proportional to the number of created electron holes, which is in turn depending on the local E-field intensity, at the site of the atom. The angular dependent measurement of fluorescence yield and crystal reflectivity can, therefore, serve to determine the position of an atom relative to the (hkl) diffraction planes.

By applying the Fourier expansion of a 3-dimensional periodic density function for the fluorescence selected atoms one can show /9/, that the H-Fourier component of the corresponding atomic distribution function can be determined. In the two-beam case, the atomic arrangement parallel to the diffraction

planes remains unknown from one measurement. Hence, additional XSW measurements /10,11/ are necessary to determine the entire atomic arrangement in three dimensions. The diffraction phenomena for x-rays, however, are not restricted to diffraction in 2-beam cases. Several diffracted beams can originate from a single incident beam when the appropriate conditions are satisfied /12/. Diffraction in multi-beam cases becomes practical when the continuous, in angle strongly collimated synchrotron radiation spectrum is used /13/.

For example, if the crystal reflection angle is tuned to satisfy a 3 beam case condition, which means that the Ewald sphere passes through points 0, G and H, the Bloch wave like photon state consists of three partial waves with wave vectors $\underline{K}_0$, $\underline{K}_G$ and $\underline{K}_H$. Their interference pattern can be described by two simultaneously excited wavefields with periodicities in direction $\underline{G}$, and $\underline{H}$. Therefore, 3-beam XSW measurements determine simultaneously, relative to the same origin in reciprocal space, two independent Fourier components of the atomic distribution function. In this paper we report 3-beam XSW experiments in Germanium and show how to use the dynamical theory to evaluate the data.

2. Three-Beam Case Dynamical Theory

Multi-beam diffraction of x-rays is described by the dynamical theory /1,12/. When the geometrical conditions are chosen such that three strong beams are excited inside a crystal, the fundamental equations which treat the coupling of the waves 0, G and H can be written as:

$$\begin{aligned} 2\nu_0 E_0 &= \chi_{0-0} E_0 + \chi_{0-G} E_G + \chi_{0-H} E_H \\ 2\nu_G E_G &= \chi_{G-0} E_0 + \chi_{G-G} E_G + \chi_{G-H} E_H \\ 2\nu_H E_H &= \chi_{H-0} E_0 + \chi_{H-G} E_G + \chi_{H-H} E_H \end{aligned} \qquad (1)$$

where $2\nu_l = (K_l^2 - k^2)/k^2$ is the "Anregungsfehler", $\chi(r) = \sum_l \chi_l \exp(-2\pi i \underline{L}\cdot\underline{r})$ is the electrical susceptibility, $\underline{E}$ is the electrical field vector and $\underline{k}$ the wave vector in vacuum.

The spatial dependence of the electrical field vector as a function of position $\underline{r}$ at a fixed reflection geometry θ, φ is expressed as:

$$E_l(\underline{r}) = \underline{E}_l \exp(-2\pi i \underline{K}_l \cdot \underline{r}) \qquad (2)$$

with

$$l = 0, G, H \quad .$$

$\underline{K}_l$ is a wave vector inside the crystal satisfying the Bragg condition

$$\underline{K}_l = \underline{K}_0 + \underline{L} \quad . \qquad (3)$$

G, H are reciprocal lattice vectors to lattice points G and H.

The local intensity of the x-ray interference field is given as:

$$|\underline{E}(\underline{r})|^2 = |\underline{E}_0 \exp(-2\pi i \underline{K}_0 \cdot \underline{r}) + \underline{E}_G \exp(-2\pi i \underline{K}_G \cdot \underline{r}) + \underline{E}_H \exp(-2\pi i \underline{K}_H \cdot \underline{r})|^2 \qquad (4)$$

with (3) follows:

$$\begin{aligned} |\underline{E}(\underline{r})|^2 = {} & |\underline{E}_0|^2 + |\underline{E}_G|^2 + |\underline{E}_H|^2 \\ & + 2\,\mathrm{Re}\,(\underline{E}_0 \underline{E}_G^* \exp(-2\pi i \underline{G}\cdot\underline{r})) \\ & + 2\,\mathrm{Re}\,(\underline{E}_0 \underline{E}_H^* \exp(-2\pi i \underline{H}\cdot\underline{r})) \\ & + 2\,\mathrm{Re}\,(\underline{E}_G \underline{E}_H^* \exp(-2\pi i (\underline{H}-\underline{G})\cdot\underline{r})) \end{aligned} \qquad (5)$$

this total wave field is periodic in the directions of G, H and (G-H). Therefore, phase and intensity of the x-ray standing wavefield is constant for all points in real space lying on the intersections of the planes defined by $\underline{G}\cdot\underline{r}$ = const and $\underline{H}\cdot\underline{r}$ = const. Therefore, the fluorescence yield in an XSW experiment will depend on the position of this line in the unit cell but is the same for any place along this line. This shows that atomic positions can simultaneously be determined in two spatial dimensions. For the simplest case, that just one atomic site is occupied, this leaves only the distribution along the line unknown.

The fundamental equations (1) can be solved by numerical methods /12,14/. It is customary to decompose the wavefields into σ and π components transforming the fundamental equations into a scalar form of a 6x6 matrix equation. In the present experimental study a diffraction geometry was chosen in which the incident wave was diffracted by two sets of diffraction planes, G and H, where the G diffraction planes were lying parallel to the crystal surface. Since Bragg-Bragg geometry is realized the incident and diffracted waves intersect the same crystal surface and each wavefield consists of two permitted modes. In our calculation of the electric fields and wavevectors inside the crystal the σ and π components and the two permitted modes of the wavefields are considered.

Including the polarisation state decomposed in σ and π components /11/ gives for the $\underline{E}$-field (E=G,H)

$$\underline{E}_E = (E_E^{\pi}(\pi) + E_E^{\pi}(\sigma))\hat{\pi}_E + (E_E^{\sigma}(\pi) + E_E^{\sigma}(\sigma))\hat{\sigma}_E \qquad (6)$$

with $\hat{\pi}_E = \underline{E}_E^{\pi}/|\underline{E}_E^{\pi}|$, $\hat{\sigma}_E = \underline{E}_E^{\sigma}/|\underline{E}_E^{\sigma}|$ and the character in brackets describing

the state of the exciting photon. Including further the case of two excited modes, gives e.g. in the case of the $E_L^{\pi}(\pi)$ component

$$E_L^{\pi}(\pi)(\underline{r}) = \sum_{j=1}^{2}\lambda_{\pi}(j)(E_L^{\pi}/E_0^{\pi})_j \exp(-2\pi i(\underline{K}_L - k\delta_j\hat{z})\cdot\underline{r}) \qquad (7)$$

with $\underline{K}_{0,j} = \underline{k} - k\delta_j\hat{z}$) and eigenvalues $\delta_j = \delta_j' + i\delta_j''$ from (1), $\hat{z}$ being the inward crystal surface normal and coefficients λ describing the correlation between σ and π components. Equivalent equations hold for the other components and determine via (6) the G, H fields.

Since the two permitted branches of the dispersion surface are almost parallel in the present case, $\delta_1' = \delta_2' = \delta'$ has been used for the numerical calculation and (7) becomes:

$$E_L^{\pi}(\pi)(\underline{r}) = \exp(-2\pi i(\underline{K}_L - k\hat{z}\delta')\cdot\underline{r}) \sum_{j=1}^{2}\lambda_{\pi}(j)(E_L^{\pi}/E_0^{\pi})_j \exp(-2\pi k\delta_j''\hat{z}\cdot\underline{r}) \qquad (8)$$

The normalized fluorescence yield $Y(\underline{r},\Theta,\varphi)$ from fluorescence selected atoms with an atomic distribution function $\rho_{fl}(\underline{r})$ can be calculated with (4), (6) and (7):

$$Y(\underline{r},\Theta,\varphi) = \int_{\text{Volume}} |E(\underline{r},\Theta,\varphi)|^2/|\underline{E}_0|^2 \, \rho_{fl}(\underline{r})\,d\underline{r} \qquad (9)$$

$\rho_{fl}(\underline{r})$ is periodic with the crystal lattice /9/ and can be expanded in a Fourier series. Accordingly the (hkl)-Fourier component is written as:

$$f_{hkl} = |f_{hkl}| \exp(2\pi i\Phi_{hkl}) \qquad (10)$$

$|f_{hkl}|$ is called coherent fraction and Φ_{hkl} coherent position of the (hkl)-component.

Inserting (9) in (8) gives, where constant A includes geometrical parameters

$$Y(\underline{r},\Theta,\varphi) = A\{(1-|\Gamma_G|)(1+|\underline{E}_G|^2/|\underline{E}_0|^2)$$

$$+ |\Gamma_G||\underline{E}_0+\underline{E}_G \exp(2\pi i\Phi_G)|^2/|\underline{E}_0|^2 + (1-|\Gamma_H|)(1+|\underline{E}_H|^2/|\underline{E}_0|^2)$$

$$+ |\Gamma_H||\underline{E}_0+\underline{E}_H \exp 2\pi i\Phi_H)|^2/|\underline{E}_0|^2 - |\Gamma_{G-H}|(|\underline{E}_H|^2/|\underline{E}_0|^2 + |\underline{E}_G|^2/|\underline{E}_0|^2)$$

$$+ |\Gamma_{G-H}| |\underline{E}_H+\underline{E}_G \exp(2\pi i\Phi_{G-H})|^2/|\underline{E}_0|^2 - 1 \} \qquad (11)$$

Therefore, a 3-beam XSW analysis depends on coherent fractions $|\Gamma_G|$, $|\Gamma_H|$ and $|\Gamma_{G-H}|$ and coherent positions Φ_G, Φ_H and Φ_{G-H}.

The effect of re-absorption of fluorescence photons inside the Ge crystal on the normalized fluorescence yield can be expressed as:

$$Y(\underline{r},\Theta,\varphi,\alpha) = \int_{\text{Volume}} |\underline{E}(\underline{r},\Theta,\varphi)|^2/|\underline{E}_0|^2 \rho_{ff}(\underline{r}) \exp(-\mu_{out}\underline{\hat{r}}\cdot\underline{r}/\sin\alpha)d\underline{r} \qquad (12)$$

where μ_{out} is the linear absorption coefficient of the fluorescence radiation in the crystal and the angle α of emittance defines the take-off angle between the crystal surface and the direction of the fluorescence radiation when leaving the crystal.

In general the wavevector $\underline{K}_i$ is a complex quantity with $\underline{K}_i = \underline{K}_i' + i\underline{K}_i''$. The imaginary part K_i'' accounts for absorption. Thus the wavevectors $\underline{K}_0$, $\underline{K}_G$ and $\underline{K}_H$ in (2), (4), (6) and (11) are complex quantities and (10) has been solved by numerical integration taking both the reabsorption of fluorescence radiation and the primary absorption and extinction of the wave into account.

3. Experiment and Results

The measurements were done with the instrument ROEMO /4,15,16/ at the Hamburg Synchrotron Radiation Laboratory HASYLAB with synchrotron radiation from the storage ring DORIS. The continuous energy spectrum and the high brilliance of the source were very advantageously used in this experiment. Before the radiation impinges on the sample crystal, a narrow energy band is chosen from the white spectrum by a slightly dispersive double crystal monochromator (Fig. 1). This vertically reflecting monochromator is composed of a symmetrical Ge(440) crystal and an asymmetrical Si(333) crystal cut with an asymmetry angle of 21.5° to reduce the transmitted vertical divergence. This combination of different crystal materials and of reflections with unmatched harmonic spectrum /17/ eliminates all problems with higher reflection orders. In the experiment, the monochromator selected a narrow energy band ΔE_γ = 1.5 eV at E_γ = 12.8 keV with an emittance angle $\Delta\Theta$ = 1.6 µrad. A narrow slit (S3) reduced the horizontal divergence of the radiation to 30 µrad. The sample was a Syton polished Ge(111) single crystal sized 18x18x6 mm^3. A Ge(000)(333)(115) 3-beam case with Bragg-Bragg geometry was chosen for the experiments. The (333) diffraction planes were aligned parallel to the crystal surface and the (115) diffraction planes were inclined relative to the crystal surface with an asymmetry angle of 30.9°. Since $d_{333} = d_{115}$ and since the lattice constants of Si (monochromator) and Ge (sample) are only slightly different, dispersion effects were neglected for the data analysis.

A series of XSW data were recorded by rotating the crystal around the [333] direction in increments of the angle φ. At each φ a measurement was carried

out in an energy dispersive mode /7,18/ by rocking both monochromator crystals in a parallel fashion through the 3-beam case range of the sample crystal, and thus scanning the photon energy. Two NaI(Tl)-detectors were used for the simultaneous registration of the (333) and (115) rocking curves. An energy dispersive Si(Li) detector collected the Ge K_α fluorescence radiation from the sample crystal. Results of a series of XSW experiments are shown in Figs. 2 and 3.

In Fig. 2.1 (a) the angular positions of the (333)- and (115)-rocking curves are clearly different. The corresponding Ge K_α fluorescence yield (Fig. 2 (a)) shows two distinct structures where the structures on the low and high angle side are related to the (333), (115) reflection, respectively. Increasing angle φ by increments of 20 µrad (Fig. 2 (a) to (f)) shows that both rocking curves first overlap and then separate again. The corresponding structures in the fluorescence yield behave accordingly. Figs. 2 (c) and (d) are close to the case when the Bragg condition is simultaneously fulfilled and the angular positions of the rocking curves overlap fully. Note, that due to conservation of energy, the (115) rocking curve shows a dip in case the (333) reflection is excited simultaneously. The corresponding Figs. 2.2 (c), (d) demonstrate that the 3-beam case X-ray standing wavefield is not simply an addition of intensities of the wavefields. When the angle is increased by further increments, the rocking curves separate again (Fig. 2 (f)), and the fluorescence yield curve splits again into two distinct structures (Fig. 2.2 (f)). Here the sequence of reflections is reversed in comparison to Fig. 2 (a). Fig. 3 shows a similar ($\Delta\varphi$ = 20 µrad) sequence when the sweep range is centered on the (333) rocking curve. While the full φ sweep range in Fig. 2 is 132 µrad it is only 41 µrad in Fig. 3, showing the 3-beam interference on an expanded scale.

4. Data Analysis and Discussion

Since the atomic arrangement inside an ideal Ge crystal is well known, the Fourier components (10) of the atomic distribution function can be calculated. Assumption of a symmetrical electron density around the nuclei gives the coherent fraction $|f_{333}| = 2^{-1/2}$ and the coherent position $\Phi_{333} = 1$, $|f_{115}| = 2^{-1/2}$ and $\Phi_{115} = 1$ and for the forbidden $(22\bar{2})$- reflection $|f_{22\bar{2}}| \cong 0$. For Ge(000)(333)(115) the interference between the 0, G and the 0, H waves contribute therefore much more to the normalized Ge K_α fluorescence yield in (11) than the G-H term.

Measurements displayed in Fig. 2 (a), (c) and (e) are chosen as examples to compare the theoretical rocking curves and fluorescence yield with measured data. The angular scales of the rocking curves are determined by a χ^2-fit of the experimental reflectivity curves to the theoretical calculation which was also convoluted with the monochromator emittance. In calculating the fluorescence yield, we used the Fourier components of the atomic distribution function and convoluted with the monochromator angular emittance.

The calculated reflectivities of the (115)- and (333)-reflections are shown in Fig. 2.1 (a) and agree very well with the measured data. Fig. 4 shows measured fluorescence yield (from Fig. 2.2 (a)) together with the fluorescence yield calculated for different emittance angle α. When α is increased, the influence of extinction and reabsorption on the fluorescence yield increases causing a smearing of the fluorescence yield curve. For $\alpha = 10''$ a satisfactory agreement is reached between experimental data and calculated curve /19/.

Such agreement is also reached for the result of a χ^2-fit of the experimental reflectivities, to the theory shown in Figs. 2 (c) and (e). The calculation of the corresponding fluorescence yield (α = 10°) in the central 3-beam case is shown in Fig. 2.2 (c). Although the theoretical reflectivity curves agree well with the experimental data, the calculated fluorescence yield shows a similar shape but the experimental curves are broader, even though the take-off angle α is included as free fit parameter. Besides for reasons of dispersion and finite angular apertures, this can additionally be caused by the non-spherical distribution of the electrons around the nuclei in germanium /20/ which causes a non vanishing (222)-Fourier component of the atomic distribution function. Therefore, the maximum of the x-ray interference field will not coincide with the maximum of the (222)-Fourier component of the atomic distribution function in real space which results in a phase shift between the interference field and the (222)-Fourier component of the atomic distribution function[5]. Thus the contribution of the interference term of the G- and H-wavefields in (8) have to be included in the calculation for further improvement.

When an x-ray standing wavefield analysis is carried out to determine an unknown atomic density distribution, the Fourier components of the atomic distribution function will be determined by a χ^2-fit of measured and calculated fluorescence yield with coherent positions and fractions as free parameters. A demonstration of the strong correlation between the position and the shape of the yield curve is given by comparing the calculated fluorescence yield for the case that atoms are located between the (333) and (115) diffraction planes (solid line in Fig. 4). Using $|f_{333}| = |f_{115}| = 2^{-1/2}$, $|f_{222}| = 0$ and $\Phi_{333} - \Phi_{115} = 1/2$, the drastic difference is clearly visible. This shows, that a two dimensional position determination can be done even close to the 3-beam condition.

Summary

The present study demonstrates that 3-beam XSW measurements can be done with synchrotron radiation. This opens the way for a two dimensional determination of atomic positions in the bulk and on the surface. For many applications, measurements close to the 3-beam case condition will suffice. For this situation, very good agreement was reached between the theoretical calculations and experimental results.

In the central region of the 3-beam case, however, all interference fields have to be included in the analysis in most reflection cases. Although such situation may be avoided for a direct position analysis, it can, however, lead to an even more detailed analysis of the charge distribution. This subject is beyond the scope of the present paper, just as the extension of the measurement to 4-beam cases which can provide more complete position analyses.

Acknowledgement

One of us (N.G.) gratefully acknowledges discussions about multiple diffraction theory with S.-L. Chang in the early stages of this project.

References

1. v. Laue, M.: Röntgenstrahlinterferenzen, Frankfurt/Main, Akademische Verlagsanstalt (1960)
2. Pinsker, Z.G.: Dynamical scattering of X-Rays in Crystals, Berlin, Heidelberg, New York, Springer-Verlag (1977)
3. Golovchenko, J.A., Batterman, B.W., Brown, W.L.: Phys. Rev. B 10, 4239 (1974)
4. Materlik, G., Zegenhagen, J.: Phys. Lett. 104 A, 47 (1984)
5. Bedzyk, M.J., Materlik, G.: Phys. Rev. B32, 6456 (1985)
6. Cowan, P.L., Golovchenko, J.A., Robbins, M.L.: Phys. Rev. Lett. 44, 1680 (1980)
7. Funke, P., Materlik, G.: Solid State Commun. 54, 121 (1985)
8. Materlik, G.: Z. Phys. B - Condensed Matter 61, 405 (1985)
9. Merlel, N., Materlik, G., Zegenhagen, J.: Z. Phys. B Condensed Matter 58, 199 (1985)
10. Golovchenko, J.A., Patel, J.R., Kaplan, D.R., Cowan, P.L., Bedzyk, M.J.: Phys. Rev. Lett. 49, 560 (1982)
11. Materlik, G., Frahm, A., Bedzyk, M.J.: Phys. Rev. Lett. 52, 441 (1984)
12. Chang, S.-L.: Multiple Diffraction of X-Rays in Crystals, Berlin, Heidelberg, New York, Springer-Verlag (1984)
13. Graeff, W. and Bonse, U.: Z. Phys. B 27, 19 (1977)
14. Hümmer, K., Billy, H.W.: Acta Cryst. A 38, 841 (1982)
15. Krolzig, A., Materlik, G., Zegenhagen, J.: Nucl. Instr. Meth. 208, 613 (1982)
16. Krolzig, A., Materlik, G., Swars, M., Zegenhagen, J.: Nucl. Instr. Meth. 219, 450 (1984)
17. Bonse, U., Materlik, G., Schröder, W: J. Appl. Cryst. 9, 223 (1976)
18. Funke, G., Materlik, G., Reimann, A.: Nucl. Inst. Meth. A246, 765 (1986)
19. Note, that no finite solid angle of emission has been included in this concept.
20. Roberto, J.B., Batterman, B.W., Keating, D.T.: Phys. Rev. B 9, 2590 (1974)

Figure Captions

Fig. 1 Experimental arrangement (schematic). S1-S5: beam collimators. X1, X2: monochromator crystals. I1, I2: ionisation chambers.

Fig. 2 3-beam Ge(000)(333)(115) results relative to the (115) rocking curve. Left row (2.1): experimental (ooo: (115); ●●●: (333)) and theoretical (— —) reflectivity curves. Right row (2.2): experimental Ge K_α fluorescence yield curves and theoretical curves (---) using a take-off angle $\alpha = 10°$ (see text). From (a) to (f) angle φ is incremented by 20 µrad.

Fig. 3 3-beam Ge(000)(333)(115) results relative to the (333) rocking curve. Left row: ooo: (115) reflection, ooo: (333) reflection. Right row: Ge K_α fluorescence yield. From (a) to (j) angle φ is incremented by 20 µrad.

Fig. 4 Experimental Ge K_α fluorescence yield (···) close to Ge(000) (333) (115) 3-beam case. (---, ----) : theoretical calculation for different take-off angles α from substitutional Ge atoms. (——): theoretical calculation for $\alpha = 0°$ and interstitial Ge atoms; Θ_B^{333}: (333) Bragg angle according to Bragg's law.

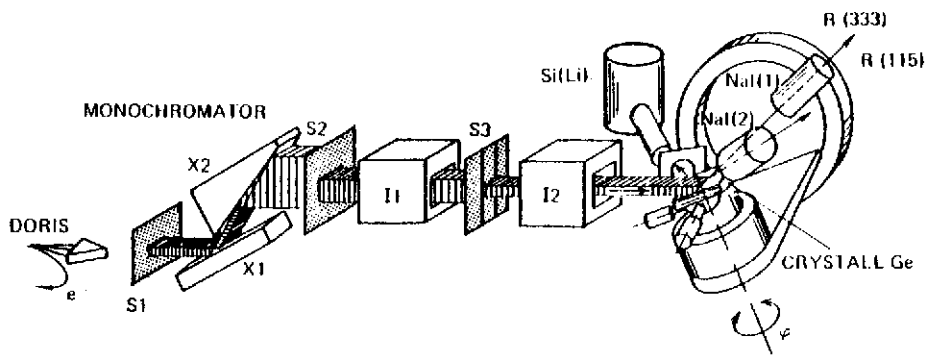
MONOCHROMATOR
DORIS
e
S1
X2
X1
S2
I1
S3
I2
Si(Li)
NaI(1)
NaI(2)
R (333)
R (115)
CRYSTALL Ge
φ

Fig. 1

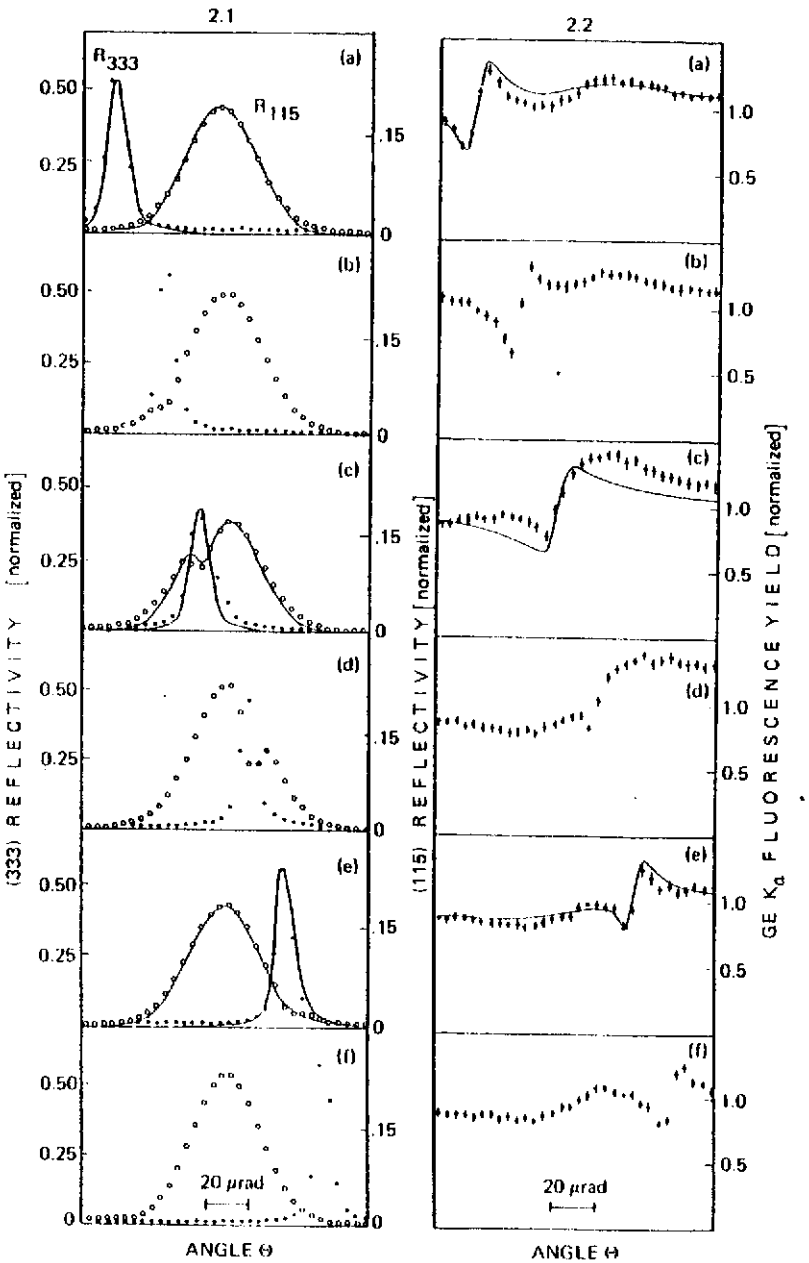
2.1
2.2
(a)
(b)
(c)
(d)
(e)
(f)
R_{333}
R_{115}
0.50
0.25
0
.15
1.0
0.5
20 μrad
(333) REFLECTIVITY [normalized]
(115) REFLECTIVITY [normalized]
GE K_α FLUORESCENCE YIELD [normalized]
ANGLE Θ

Fig. 2

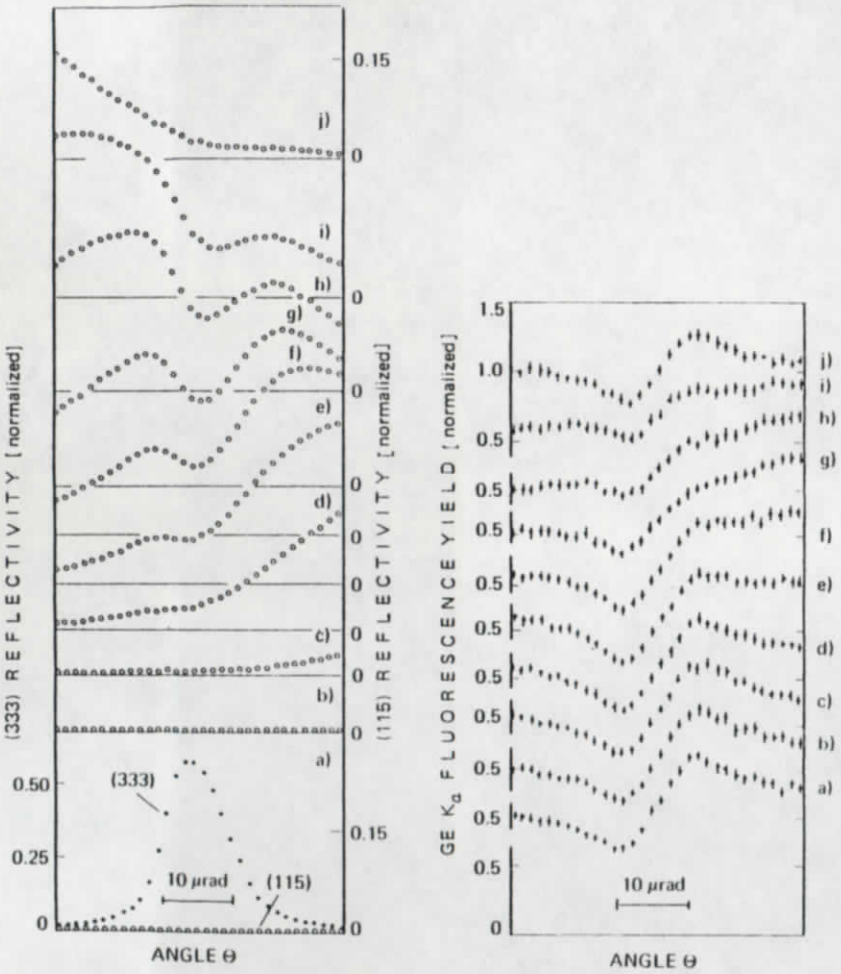
(333) REFLECTIVITY [normalized]
(115) REFLECTIVITY [normalized]
GE K_α FLUORESCENCE YIELD [normalized]
ANGLE θ
(333)
(115)
10 μrad
a)
b)
c)
d)
e)
f)
g)
h)
i)
j)

Fig. 3

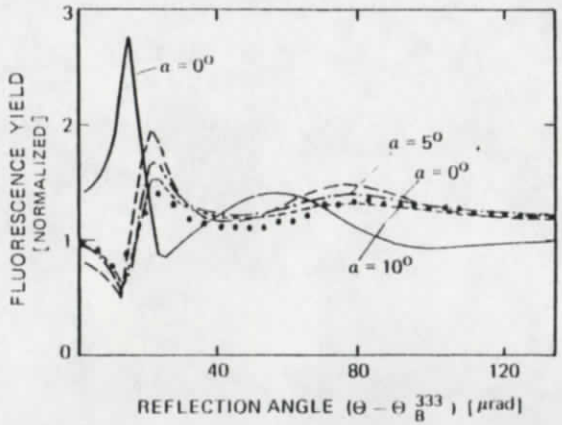
FLUORESCENCE YIELD
[NORMALIZED]
REFLECTION ANGLE (θ − θ $^{333}_{B}$) [μrad]
α = 0°
α = 5°
α = 0°
α = 10°

Fig. 4